Colloids and Surfaces B: Biointerfaces 109 (2013) 212–218

Contents lists available at SciVerse ScienceDirect

Colloids and Surfaces B: Biointerfaces

journal homepage: www.elsevier.com/locate/colsurfb

Hard corona composition and cellular toxicities of the graphene sheets

Hongying Mao[a,**], Wei Chen[a,b], Sophie Laurent[c], Coralie Thirifays[c], Carmen Burtea[c], Farhad Rezaee[d], Morteza Mahmoudi[e,f,*]

[a] Department of Chemistry, National University of Singapore, 2 Science Drive 3, 117543, Singapore
[b] Department of Physics, National University of Singapore, 3 Science Drive 3, 117542, Singapore
[c] Department of General, Organic, and Biomedical Chemistry, NMR and Molecular Imaging Laboratory, University of Mons-Hainaut, Avenue Maistriau, 19, B-7000 Mons, Belgium
[d] Department for Experimental and Molecular Medicine, Academic Medical Center, University of Amsterdam, Amsterdam, The Netherlands
[e] Department of Nanotechnology, Faculty of Pharmacy Tehran University of Medical Sciences, P.O. Box 14155-6451, Tehran, Iran
[f] Nanotechnology Research Center, Faculty of Pharmacy, Tehran University of Medical Sciences, P.O. Box 14155-6451, Tehran, Iran

ARTICLE INFO

Article history:
Received 2 November 2012
Received in revised form 13 March 2013
Accepted 27 March 2013
Available online 9 April 2013

Keywords:
Graphene-sheets
Nanotoxicology
Protein corona
ROS
Confocal microscopy

ABSTRACT

Graphene nanomaterials are recognized as one of the most promising nanomaterials because of their unique and highly attractive physicochemical properties (e.g., thermal conductivity, superlative mechanical strength, and ultrahigh surface-to-volume ratios). It is well established that when nanomaterials interact with biological medium, biomolecules and in particular proteins attach to their surfaces, which form a complex between surface of nanoparticles and proteins called corona. Thus, the interaction of the biological system with the nanomaterials depends on the composition of the protein layer, rather than the surface characteristics of the nanomaterials itself. Although there is a significant increase of interest in the application of graphene in medical science, there has been a little attention to the nanotoxicological aspects of these newly developed materials. For this reason, we aimed to investigate whether the effect of the interactions between graphene-sheets with various human plasma concentrations (i.e. both in vitro (cells/tissues) and in vivo simulating states) is toxic. The results showed that by increasing the human plasma concentration, the affinity of proteins with low molecular weights to graphene-sheets surface is significantly increased. Fluorescence microscopy of Hela and Panc-1 cell lines showed a reduction of nuclei number and an increase of reactive oxygen species (ROS) production respectively after a longer incubation of graphene-sheets with plasma proteins. ROS production was higher in Panc-1 cell line, when used as protein source for graphene-sheets than HeLa cell line.

1. Introduction

During last decade, there has been an intense focusing on the carbon-based nanomaterials (i.e. fullerene, nanodiamond, and carbon nanotubes (both single- and multi-walled)). The reason for a high interest in carbon-based nanomaterials is due to their several unique properties that maintain various potential applications in medicine such as drug delivery, transfection imaging, biosensing, and photothermal therapy [1–10]. The new member of carbon-based nanomaterials family is graphene. Graphene as a two-dimensional sheet of sp^2-hybridized carbon atoms in a closely packed honey comb lattice is one of the most promising nanomaterials because of its unique properties such as high carrier mobility, unparalleled thermal conductivity, superlative mechanical strength, and ultrahigh surface-to-volume ratios [11]. After the first single-layer graphene sample was prepared by Geim and co-workers in 2004 by mechanical exfoliation of small mesas of highly oriented pyrolytic graphite, lots of other methods have been developed to synthesize graphene, including chemical vapor deposition (CVD) on thermally annealed copper/nickel foil, epitaxial growth on SiC, thermal annealing of a ruthenium single crystal containing carbon, unzipping of carbon nanotube, and solution based reduction of graphene oxide (GO) [12,13]. In addition, functionalized graphene and GO have also received extensive attentions and as evidence, the biocompatibility, solubility, selectivity and conductivity being further improved [14–17].

Although the number of graphene-related publications has been generally increased over the years, majority of the reports are focused on the physico-chemical properties of graphene such as synthesis, characterization, surface properties, electrical and optical properties. However, there are a few studies, compared to the synthesis and preparation reports, about the toxicity of graphene

* Corresponding author. Current address: School of Chemical Sciences, University of Illinois at Urbana-Champaign, 600 South Mathews Avenue, Urbana, Illinois 61801, United States.
** Corresponding author.
E-mail addresses: chmmh@nus.edu.sg (H. Mao), Mahmoudi@illinois.edu, mori.mahmoudi@yahoo.com (M. Mahmoudi).

0927-7765/$ – see front matter © 2013 Elsevier B.V. All rights reserved.
http://dx.doi.org/10.1016/j.colsurfb.2013.03.049

and its derivatives [1]; therefore, a significant knowledge gap exists on a complete toxicological profile of these promising nanomaterials proposed for safe use in future in many aspects of biomedical engineering. The lack of this toxicological knowledge hampers the risk assessment or regulation for safety application of the materials.

It is now well-recognized that the surfaces of biomaterials (e.g., implants and medical devices) and nanomaterials (e.g., nanoparticles, dendrimers, nanotubes, and nanofilms) are immediately attracting biomolecules (e.g., proteins, natural organic materials, detergents, and enzymes) upon their contact with a biological system [18]. These biomolecules coated surfaces confer a new "biological identity" in the biological environment, which determines the subsequent cellular/tissue responses [19–25]. Therefore, what a biological system (such as cells, tissues and organs) so-called "sees" when interacting with graphene sheets appeared to be completely different from the original pristine surface of the graphene sheets.

Here, we investigated the toxicological effect of the interaction between protein source and the surface of graphene sheets. Graphene–protein complexes have been evaluated by atomic force microscopy (AFM), Raman spectroscopy, one-dimensional sodium dodecyl sulfate polyacrylamide gel electrophoresis (1-DE approach (SDS-PAGE)) and electrospray liquid chromatography mass spectrometry (LC MS/MS). The results clearly confirmed existence of complex interactions between graphene sheet and proteins. In addition, we have also determined toxicity state of graphene sheets and mammalian cells (as protein suppliers) interaction.

2. Materials and methods

2.1. Synthesis of graphene sheets

The growth of CVD graphene was carried out in a quartz tube at reduced pressure state. In order to obtain copper crystal with larger grain size, copper foil (25 μm thick, 99.999% purity) was annealed at 1000 °C for 30 min under a combined flow of Ar:H_2 = 50:10 (10 sccm) before the growth of graphene with a pressure of approximately 0.2 Torr. During the growth, a high purity of methane (99.999%, 30 sccm) was introduced to the quartz tube together with Ar:H_2 (10 sccm) and the pressure was approximately 0.4 Torr. After 30 min of growth, the system was cooled down to room temperature under Ar:H_2 (10 sccm).

2.2. Interaction of graphene-substrate with plasma protein

In order to probe the formation and type of associated proteins at the surface of graphene-substrate, the graphene-substrates were fitted on polystyrene wells and plasma proteins (PP) with various concentrations (i.e. 2.5, 5, 10, 20, 30, 40, 50, 60, and 70% of total plasma proteins) were added to the substrate. Specifically, 900 μl of plasma proteins was added to each graphene-substrate and the mixture was incubated at 37 °C for 1 h. Since the previous studies reported that the protein corona is formed in a relatively stable manner over a period of 1 h [26], we have selected 1 h for evaluation of protein coronas in our samples. In order to maintain the "hard corona" composition at the surface of graphene-substrates, we have carefully removed the supernatant from graphene-substrates followed by washing with 500 μl of phosphate buffer saline (PBS) and the fraction removed. It must be noted that the washing process was designed to remove the excess of free proteins. Finally, the washed substrates were washed by 500 μl of 0.1 M of KCl solutions for proteins detachment and stored for hard corona assessments. Notably, the proteins were stored in non-sticky tubes (Eppendorf).

2.3. Cell culture and treatments

PANC-1 (Human pancreatic carcinoma, epithelial-like cell line) cells were cultured in pyruvate-free DMEM culture medium supplemented with 10% horse serum, non-essential aminoacids and penicillin/streptomycin (all from Invitrogen, Merelbeke, Belgium). HeLa (human cervical epithelial adenocarcinoma) cells were cultured in RPMI culture medium supplemented with 10% fetal bovine serum, and penicillin/streptomycin (all from Invitrogen).

The cells were seeded on coverslips before incubating them for 4 h or 24 h with graphene samples of about 15 mm^2, which was placed carefully beside the coverslip, inside the wells of the 12-well culture plate. For microscopy, the cultured cells were mounted on microscope slides. Control cells were not incubated with graphene. Finally, the cells were washed two times with Hanks balanced salt solution (HBSS) and labeled with various fluorescent dyes as described below.

2.4. MTT cytotoxicity assay

Cytotoxicity was assessed using the MTT (3-(4,5-dimethylthiazol-2-yl)-2,5-diphenyltetrazolium bromide) assay (TOX1 In Vitro Toxicology Assay Kit, Sigma–Aldrich, Bornem, Belgium). It should be noted that modified MTT method were employed based on our previous results [27–29]. After the incubation of the cells with graphene samples, they were rinsed two times with PBS and the MTT was added to each well after diluting it to 1:10 in the culture media according to the manufacturer instructions. Following incubation for 3 h, the media was removed and formazan crystals were dissolved by incubation for 15 min in 500 μL of dimethyl sulfoxide (DMSO, Sigma–Aldrich). The absorbance of each well was read at 570 nm on a microplate reader (Stat Fax-2100, Awarness Technology, Fisher Bioblock Scientific, Tournai, Belgium), with a correction background absorbance at 690 nm. The percentage of viability was calculated as the ratio of treated cells over the negative control cells.

2.5. Reactive oxygen species (ROS) assay

The cross-talked cells-graphene was incubated for 50 min at 37 °C with 25 μM 5-(and-6)-chloromethyl-2,7-dichlorodihydrofluorescein diacetate acetyl ester (H_2DCFDA, Invitrogen) diluted in HBSS. Five minutes before ending the incubation with H_2DCFDA, a solution of Hoechst 33342 dye (Invitrogen) was added at a final concentration of 1 μM. After washing the cells two times with HBSS, they were mounted on microscope slides. All samples were observed on a DM2000 Leica microscope (Leica Microsystems, Groot Bijgaarden, Belgium) equipped with a Leica DFC 290 camera. A semi-quantitative analysis of the fluorescent labeling slides has been performed using the ImageJ analysis software (National Institutes of Health, USA). The fluorescence intensities being related to the cell number per microphotograph. The results were finally expressed as percentage of treated cells as compared to the control slides.

2.6. 1-dimensional electrophoresis (1-DE (SDS-PAGE))

2.6.1. SDS-PAGE

To profile the formed hard coronas on the surface of graphene-substrates, SDS-PAGE was employed. In this regard, the eluted proteins were further separated on 12% SDS-PAGE. The defined bands were cut and after in-gel tryptic digestion injected to LC-MS for peptide sequences.

2.6.2. Liquid chromatography mass spectrometry (LC-MS/MS)

Samples were loaded onto a nanoAcquity UPLC system (Waters) equipped with a nanoAcquity Symmetry C_{18} column, 5 μm trap (180 μm × 20 mm Waters) and a nanoAcquity BEH130 1.7 μm C_{18} capillary column (75 μm × 250 mm, Waters). The trap wash solvent was 0.1% (v/v) aqueous formic acid and the trapping flow rate was 10 μL/min. The trap was washed for 5 min before switching flow to the capillary column. The separation used a gradient elution of two solvents (solvent A: 0.1% (v/v) formic acid; solvent B: acetonitrile containing 0.1% (v/v) formic acid). The flow rate for the capillary column was 300 nL/min. Column temperature was 60 °C and the gradient profile was as follows: initial conditions 5% solvent B, followed by a linear gradient to 30% solvent B over 125 min, then a linear gradient to 50% solvent B over 5 min, followed by a wash with 95% solvent B for 10 min. The column was returned to initial conditions and re-equilibrated for 30 min before subsequent injections. The nanoLC system was interfaced with a maXis LC-MS/MS System (Bruker Daltonics) with a nano-electrospray source fitted with a steel emitter needle (180 μm O.D. × 30 μm I.D., Proxeon). Positive ESI-MS & MS/MS spectra were acquired using AutoMSMS mode. Instrument control, data acquisition and processing were performed using Compass 1.3 SR3 software (microTOF control, Hystar and Data Analysis, Bruker Daltonics). Instrument settings were: ion spray voltage: 1500 V, dry gas: 6 L/min, dry gas temperature 160 °C, ion acquisition range: *m/z* 50–2200. AutoMSMS settings were: MS: 0.5 s (acquisition of survey spectrum), MS/MS (CID with N_2 as collision gas): ion acquisition range: *m/z* 300–1500, 0.1 s acquisition for precursor intensities above 100,000 counts, for signals of lower intensities down to 1000 counts acquisition time increased linear to 1 s, the collision energy and isolation width settings were automatically calculated using the AutoMSMS fragmentation table:, 5 precursor ions, absolute threshold 1000 counts, preferred charge states: 2–4, singly charged ions excluded. 1 MS/MS spectrum was acquired for each precursor and former target ions were excluded for 30 s. Tandem mass spectral data were submitted to database searching using a locally-running copy of the Mascot program (Matrix Science Ltd., version 2.3), through the Bruker ProteinScape interface (version 2.1). All spectra were searched against the Swiss-Prot database restricted to mammalia sequences only (63,676 sequences). Search parameters specified: Enzyme; Trypsin, Peptide Mass Tolerance; 10 ppm, Fragment Mass Tolerance; 0.1, Fixed Modifications; Methylthio (C), Variable Modification; Oxidation (M). All peptide identifications were filtered to only accept expected values of 0.05 or lower. Empirically derived estimates of peptide false discovery rate are calculated from searches against a Mascot generated decoy database.

3. Results and discussion

3.1. Characterization of graphene-sheets

The Raman spectra were measured using WITEC CRM200 Raman system at room temperature. The excitation source is 532 nm laser (2.33 eV) with its power lower than 0.1 mW to avoid laser induced heating of the sample. The Raman spectra of graphene film on copper foil before and after interacting with protein (10%) are shown in Fig. 1. The inset in Fig. 1 shows the Raman spectrum for CVD graphene transferred onto oxidized Si substrates (300 nm SiO_2), which indicates that the graphene samples in our experiments are single-layer graphene as shown in Fig. 2a and b, the morphology of CVD graphene film on SiO_2 was measured by AFM with tapping mode under ambient conditions, the collected data were analyzed using the Nanoscope VI program. The average grain size of graphene is about 10 μm as shown in Fig. 2c. The scanning electron microscope (SEM) image was measured with JSM-6700F (JEOL).

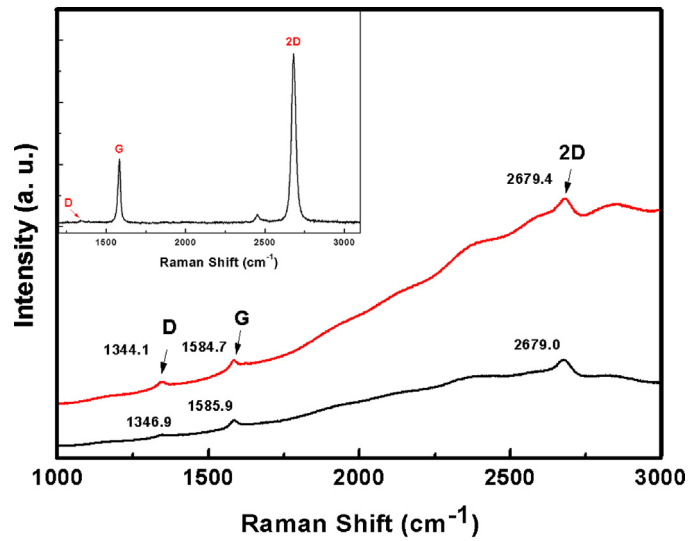

Fig. 1. The Raman spectra for graphene film on copper foil before (black) and after interacting with protein (red). The inset shows the Raman spectrum for graphene film on SiO_2 (300 nm), the intensity ratio between 2D and G peaks together with the full width at half maximum (FWHM) of 2D peak (28.0 cm^{-1}) indicates that the CVD graphene sample in our experiments is single-layer graphene. After the modification of protein, there is nearly no shift for both 2D and G peak, while the intensity of defect related D peak increases.

3.2. Protein corona

To make it possible to see a high degree of confidence in the view of the hard protein corona in a biological state, we examined and evaluated various protein concentrations and their attachment on the surfaces of graphene-substrates using 1-DE-LC-MS/MS. As depicted in Figs. 3 and 4, the relative intensities and location of the protein bonds are strongly dependent on the protein concentrations.

Based on the results obtained by SDS-PAGE as displayed in Fig. 3, the proteins with a molecular weight of approximately 72 kDa appeared to be interacted with graphene-substrates at a low concentration of proteins (i.e. 2.5–20%), whereas, several additional bands were detected at higher protein concentrations (i.e. 30–70%). Interestingly, with the increase of protein concentrations, the tendency of proteins with lower molecular weight for cross-react with hard corona composition was significantly enhanced as compared with proteins of approximately 72 kDa. After treatment of graphene-sheet with 70% plasma proteins, a few proteins were detected with a higher molecular weight as compared with 72 kDa band as shown in Figs. 3 and 4. From the band intensity graphs (see Fig. 4), it is clear that the amount of surface associated proteins at the surface of graphene-substrates increased dramatically up to protein concentration of 20%. From 30 to 60% of protein interacted solutions, the amount of surface associated proteins were approximately stable followed by significant band intensity incensement at 70%. Although the state-of-art proteomics is one of the best approach to analyze the protein content in biological fluids such as human plasma/serum, the presence of very high-abundant proteins such as albumin, immunoglobin (IgG), and α2-macroglobulin hampers the analysis of medium-to-low abundant proteins in plasma/serum samples [26]. Based on the above mentioned argument, three possible explanations for our findings could be due to (1) the 72 kDa protein is highly intense because it is a very high-abundant proteins (i.e. albumin). Thus, when the concentration of proteins increases, that is then logic to conclude that the relative intensity of 72 kDa band increases too. (2) Several bands with low molecular weight, which were detected when the protein concentrations were increased and this could be due to

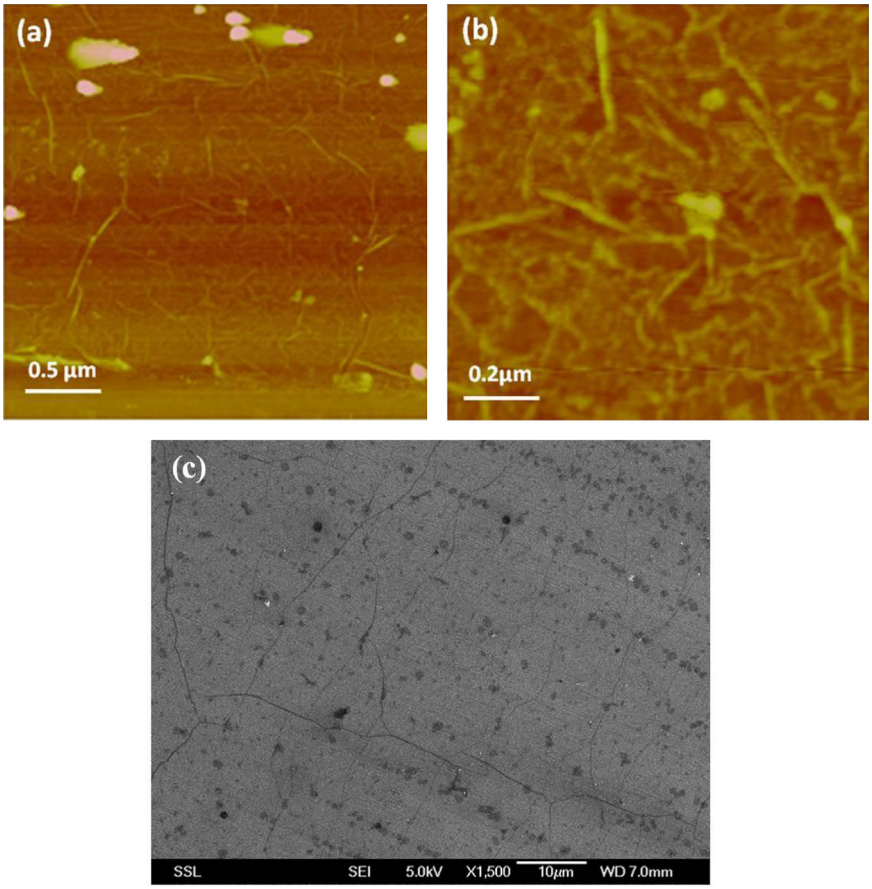

Fig. 2. AFM measurements of the CVD graphene film on SiO_2 substrate (a) 3 μm × 3 μm (b) 1 μm × 1 μm (c) SEM image of graphene on SiO_2.

the reaching of these proteins to the sensitive levels compatible to the used MS instrument and (3) another possible interpretation is that the amount of proteins associated with surface of graphene-substrates increased dramatically up to a protein concentration of 20%. From 30 to 60% of protein interacted solutions, the amount of surface associated proteins were approximately stable followed by significant band intensity incensement at 70%.

In order to obtain the total number of the MS/MS spectra for all of the peptides that are attributed to a matched protein, a semi-quantitative assessment of the protein amounts was conducted through application of spectral counting method (SpC). The normalized SpC amounts of each protein, identified in the MS study of smooth and jagged surfaces, were calculated by applying the following equation [30]:

$$\mathrm{NpSpC_k} = \left(\frac{(\mathrm{SpC}/(\mathrm{Mw})_\mathrm{k})}{\sum_{i=1}^{n} (\mathrm{SpC}/(\mathrm{Mw})i)} \right) \times 100 \quad (1)$$

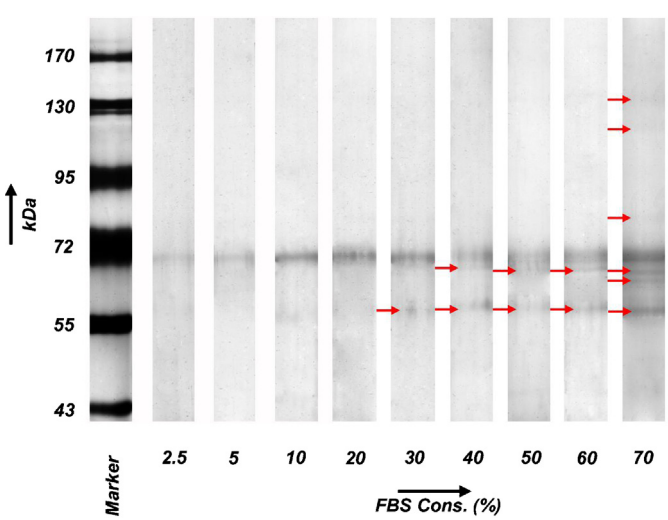

Fig. 3. SDS-PAGE gel of hard corona human plasma proteins following incubation at different plasma concentrations.

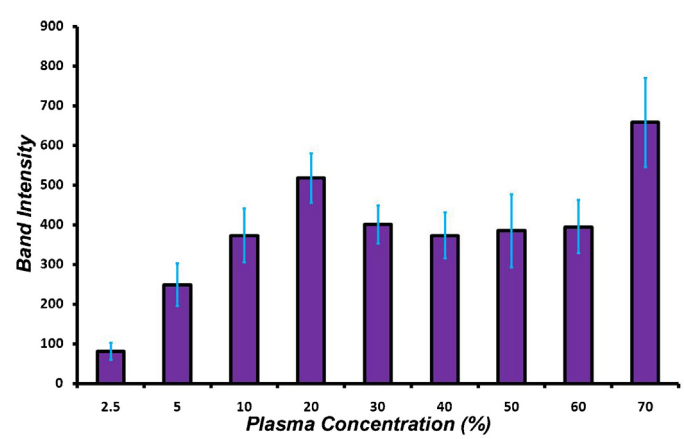

Fig. 4. Histogram representing the total band intensity of proteins recovered from hard corona human plasma proteins following incubation at different plasma concentrations.

Table 1
Hard corona proteins associated with graphene-substrates following incubation at different plasma concentrations, as identified by LC MS/MS.[a]

Gel band Mw (kDa)	Protein identity	NSpC								
		2.5	5	10	20	30	40	50	60	70
>72	Inter-alpha-trypsin inhibitor heavy chain	<0.1	<0.1	<0.1	<0.1	<0.1	<0.1	<0.1	<0.1	1.11
	Thrombospondin-1	<0.1	<0.1	<0.1	<0.1	<0.1	<0.1	<0.1	<0.1	0.96
	Complement component C7	<0.1	<0.1	<0.1	<0.1	<0.1	<0.1	<0.1	<0.1	1.87
65–72	Prothrombin	<0.1	<0.1	13.72	21.28	11.12	16.32	17.61	15.29	11.32
	Serum albumin	100	100	86.28	66.62	70.28	55.33	66.94	49.85	26.85
	aAlpha-fetoprotein	<0.1	<0.1	<0.1	12.10	5.85	7.48	5.69	11.43	8.95
	Fibrinogen alpha chain	<0.1	<0.1	<0.1	<0.1	<0.1	4.72	2.21	5.23	9.51
	C4b-binding protein alpha chain	<0.1	<0.1	<0.1	<0.1	<0.1	<0.1	<0.1	<0.1	7.53
	Kininogen-1	<0.1	<0.1	<0.1	<0.1	<0.1	<0.1	<0.1	<0.1	8.98
55–65	Vitamin D-binding protein	<0.1	<0.1	<0.1	<0.1	4.32	5.28	2.32	8.47	7.34
	Fibrinogen beta chain	<0.1	<0.1	<0.1	<0.1	8.43	10.87	5.23	9.73	6.97
	Cytochrome	<0.1	<0.1	<0.1	<0.1	<0.1	<0.1	<0.1	<0.1	8.61

[a] Normalized spectral count (NSpC) values were calculated for each protein hit according to Eq. (1).

where, $NpSpC_k$ is the normalized percentage of spectral count for protein k, SpC is the spectral count identified, and Mw is the molecular weight (in kDa) of the protein k. Using Eq. (1), it can be expected to obtain the protein size and to evaluate the real contribution of each protein to the hard corona composition [26]. Accordingly, the normalized SpC (i.e. NSpC) values for all of the proteins identified in the hard coronas (i.e. for all employed concentrations of proteins) were determined and full results were presented in Table 1. Based upon the results, serum albumin was the only attached protein at the surface of graphene-substrates for protein concentration of 2.5 and 5%. Using protein concentrations of 10% and 20%, two additional proteins were identified and added to the composition of protein coronas, including prothrombin and alpha-fetoprotein. By increasing the protein concentrations to 30%, lower molecular weight-proteins, including vitamin D-binding protein and fibrinogen beta chain were entered to the composition of protein corona. The maximum proteins attendance in the composition of protein corona was observed in protein concentrations to 70%; in this case, inter-alpha-trypsin inhibitor heavy chain, thrombospondin-1, complement component C7, prothrombin, serum albumin, alpha-fetoprotein, fibrinogen alpha chain, C4b-binding protein alpha chain, kininogen-1, vitamin D-binding protein, fibrinogen beta chain, and cytochrome were participated in protein corona composition. In this regard, it must be noted that fibrinogen and other identified proteins considered as protein contents of corona belong to the medium-abundant plasma proteins.

3.3. Cellular toxicity of graphene-sheets

It is well established that the cell type can have quite significant role in the definition of suitable pathway for detoxification of nanomaterials, which has deep implications for safe and high yield design of nanomaterials for biomedical applications [31,32]. In order to check the effect of cell type on the toxicity of the graphene-sheets, different cell lines (i.e. HeLa and PANC-1 cells) were treated with the same surface of graphene-sheets. Using MTT assay, the cell toxicity effects of the graphene-sheets were evaluated and the results (see Fig. 5a) revealed that the graphene-sheets have no toxic effects on both tested cells. Interestingly, the viability of Hela cells was even increased after a short incubation of 4 h with graphene sheet as compared to a 24 h incubation. This finding was also confirmed by fluorescence microscopy of the Hela cells as depicted in Fig. 6. On the contrary, we did not observe any effect of incubation time on PANC-1 cells using MTT approach as demonstrated in Fig. 5a. Intriguingly, fluorescence microscopy showed that ROS production was severely increased in PANC-1 cells, used as protein source for the interaction with graphene sheet for a short period of 4 h; almost all cells were in growing phase or dead after an incubation of 24 h. These results let us to conclude that the induction of toxicity by graphene sheet-protein complex is strongly dependent on cell type as protein source (Fig. 6). However, it is well known that pancreas contains a cocktail of lysis juice, which ensures the breakdown of DNA, RNA and proteins. That is then logic to assume that the ROS production

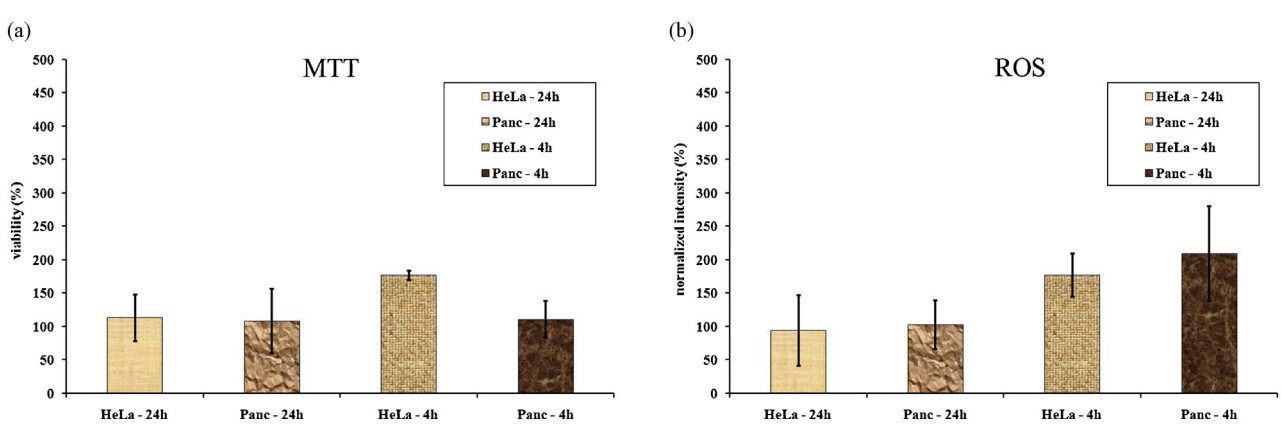

Fig. 5. (a) MTT assay results for incubated cells with the graphene-sheets (for 4 h and 24 h) from various cell lines, including Hela and Panc-1 cells; (b) fluorescence intensities of intracellular ROS for HeLa and Panc-1 cells after 4 h and 24 h treatments with graphene-sheets.

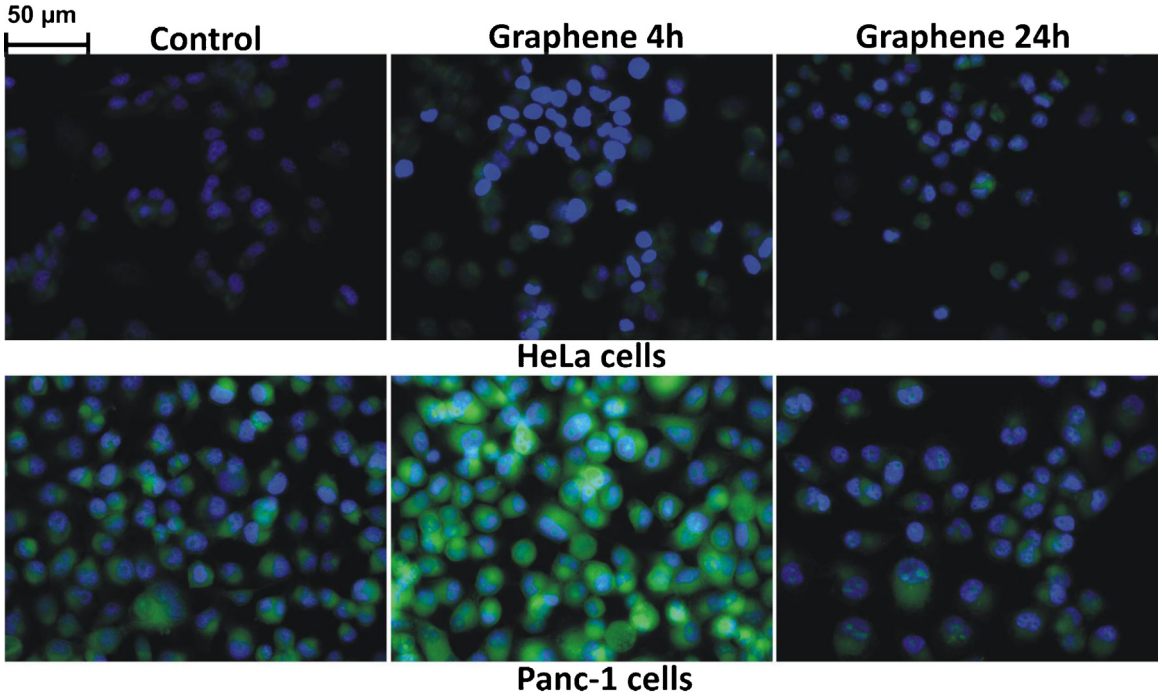

Fig. 6. Induced ROS for control cells and cells incubated with the graphene-sheets from various cell lines, including Hela and Panc-1 cells; the ROS level and nucleus are seen as green and blue fluorescence, respectively. (For interpretation of the references to color in this figure legend, the reader is referred to the web version of the article.)

in PANC-1 cell line is higher than HeLa cell line as protein source.

Since the surfaces of graphene-sheets were covered by serum albumin and prothrombin (see Table 1 for details) in 10% plasma proteins (i.e. in vitro) together with the fact that sialic acid have good capability to attach to these proteins [33,34], we expect that ROS production might be positively correlated with the amount of sialic acid content of these cells. Sialic acid is a generic term to indicate a wide family of related nine-carbon sugar acids that feature prominently at terminal positions of many eukaryotic surface-exposed glycol-conjugates, where they confer important properties upon the resulting cell surface [35]. The pancreatic cancer cell lines contain high concentrations of the sialic acid in their membrane glycoproteins, which is responsible for the negative charges on the cell surface whereas HeLa cells have lower levels of sialic acid on the cell membrane [36]. This means that pancreatic cancer cell lines may be able to interact with the graphene-sheets compared to the HeLa cells; this phenomenon is responsible for either lower cell viability amounts or higher induced ROS level in Panc-1 cells.

4. Conclusions

In this study, the protein corona and cellular toxicity of graphene-sheets were investigated. According to the results, the hard corona on the surface of graphene-substrates can evolve quite significantly as one passes from protein concentrations appropriate to in vitro cell studies to those present in in vivo studies, which has deep implications for in vitro–in vivo extrapolations and will require significant consideration in the future. The cellular responses to the graphene-sheets are strongly dependent to either cell type or hard corona composition.

References

[1] W. Hu, C. Peng, M. Lv, X. Li, Y. Zhang, N. Chen, C. Fan, Q. Huang, Protein corona-mediated mitigation of cytotoxicity of graphene oxide, ACS Nano 5 (5) (2011) 3693–3700.
[2] P. Ball, Roll up for the revolution, Nature 414 (6860) (2001) 142–144.
[3] M. Muoth, T. Helbling, L. Durrer, S.W. Lee, C. Roman, C. Hierold, Hysteresis-free operation of suspended carbon nanotube transistors, Nat. Nanotechnol. 5 (8) (2010) 589–592.
[4] D. Pech, M. Brunet, H. Durou, P. Huang, V. Mochalin, Y. Gogotsi, P.L. Taberna, P. Simon, Ultrahigh-power micrometre-sized supercapacitors based on onion-like carbon, Nat. Nanotechnol. 5 (9) (2010) 651–654.
[5] S. Bae, H. Kim, Y. Lee, X. Xu, J.S. Park, Y. Zheng, J. Balakrishnan, T. Lei, H. Ri Kim, Y.I. Song, et al., Roll-to-roll production of 30-inch graphene films for transparent electrodes, Nat. Nanotechnol. 5 (8) (2010) 574–578.
[6] C. Rutherglen, D. Jain, P. Burke, Nanotube electronics for radio frequency applications, Nat. Nanotechnol. 4 (12) (2009) 811–819.
[7] Z. Liu, W. Cai, L. He, N. Nakayama, K. Chen, X. Sun, X. Chen, H. Dai, In vivo biodistribution and highly efficient tumour targeting of carbon nanotubes in mice, Nat. Nanotechnol. 2 (1) (2007) 47–52.
[8] C.C. Fu, H.Y. Lee, K. Chen, T.S. Lim, H.Y. Wu, P.K. Lin, P.K. Wei, P.H. Tsao, H.C. Chang, W. Fann, Characterization and application of single fluorescent nanodiamonds as cellular biomarkers, Proc. Natl. Acad. Sci. U.S.A. 104 (3) (2007) 727–732.
[9] K. Welsher, Z. Liu, D. Daranciang, H. Dai, Selective probing and imaging of cells with single walled carbon nanotubes as near-infrared fluorescent molecules, Nano Lett. 8 (2) (2008) 586–590.
[10] Z. Liu, M. Winters, M. Holodniy, H. Dai, siRNA delivery into human T cells and primary cells with carbon-nanotube transporters, Angew. Chem. Int. Ed. 46 (12) (2007) 2023–2027.
[11] C.N.R. Rao, A.K. Sood, K.S. Subrahmanyam, A. Govindaraj, Graphene: the new two-dimensional nanomaterial, Angew. Chem. Int. Ed. 48 (42) (2009) 7752–7777.
[12] D. Wei, Y. Liu, Controllable synthesis of graphene and its applications, Adv. Mater. 22 (30) (2010) 3225–3241.
[13] K.S. Novoselov, A.K. Geim, S.V. Morozov, D. Jiang, Y. Zhang, S.V. Dubonos, I.V. Grigorieva, A.A. Firsov, Electric field effect in atomically thin carbon films, Science 306 (5696) (2004) 666–669.
[14] Z. Liu, J.T. Robinson, X. Sun, H. Dai, PEGylated nanographene oxide for delivery of water-insoluble cancer drugs, J. Am. Chem. Soc. 130 (33) (2008) 10876–10877.
[15] C.H. Lu, C.L. Zhu, J. Li, J.J. Liu, X. Chen, H.H. Yang, Using graphene to protect DNA from cleavage during cellular delivery, Chem. Commun. 46 (18) (2010) 3116–3118.
[16] K. Yang, S. Zhang, G. Zhang, X. Sun, S.T. Lee, Z. Liu, Graphene in mice: Ultrahigh in vivo tumor uptake and efficient photothermal therapy, Nano Lett. 10 (9) (2010) 3318–3323.
[17] H.Y. Mao, S. Laurent, W. Chen, O. Akhavan, M. Imani, A.A. Ashkarran, Mahmoudi M, Graphene: promises, facts, opportunities, and challenges in nanomedicine, Chem. Rev. (2013), http://dx.doi.org/10.1021/cr300335p, in press.
[18] M. Mahmoudi, I. Lynch, M.R. Ejtehadi, M.P. Monopoli, F.B. Bombelli, S. Laurent, Protein–nanoparticle interactions: opportunities and challenges, Chem. Rev. 111 (9) (2011) 5610–5637.

[19] D. Walczyk, F.B. Bombelli, M.P. Monopoli, I. Lynch, K.A. Dawson, What the cell "sees" in bionanoscience, J. Am. Chem. Soc. 132 (16) (2010) 5761–5768.
[20] M.P. Monopoli, D. Walczyk, A. Campbell, G. Elia, I. Lynch, F. Baldelli Bombelli, K.A. Dawson, Physical–chemical aspects of protein corona: relevance to in vitro and in vivo biological impacts of nanoparticles, J. Am. Chem. Soc. 133 (8) (2011) 2525–2534.
[21] M.P. Monopoli, F.B. Bombelli, K.A. Dawson, Nanobiotechnology: nanoparticle coronas take shape, Nat. Nanotechnol. 6 (1) (2011) 11–12.
[22] I. Lynch, A. Salvati, K.A. Dawson, Protein–nanoparticle interactions: what does the cell see? Nat. Nanotechnol. 4 (9) (2009) 546–547.
[23] M. Lundqvist, J. Stigler, G. Elia, I. Lynch, T. Cedervall, K.A. Dawson, Nanoparticle size and surface properties determine the protein corona with possible implications for biological impacts, Proc. Natl. Acad. Sci. 105 (38) (2008) 14265–14270.
[24] I. Lynch, Dawson KA, Protein–nanoparticle interactions, Nano Today 3 (1–2) (2008) 40–47.
[25] T. Cedervall, I. Lynch, S. Lindman, T. Berggård, E. Thulin, H. Nilsson, K.A. Dawson, S. Linse, Understanding the nanoparticle–protein corona using methods to quantify exchange rates and affinities of proteins for nanoparticles, Proc. Natl. Acad. Sci. 104 (7) (2007) 2050–2055.
[26] D. Walczyk, F.B. Bombelli, M.P. Monopoli, I. Lynch, K.A. Dawson, What the cell "sees" in bionanoscience, J. Am. Chem. Soc. 132 (16) (2010) 5761–5768.
[27] M. Mahmoudi, A. Simchi, M. Imani, A.S. Milani, P. Stroeve, An in vitro study of bare and poly(ethylene glycol)-co-fumarate-coated superparamagnetic iron oxide nanoparticles: a new toxicity identification procedure, Nanotechnology 20. (22) (2009).
[28] S. Laurent, C. Burtea, C. Thirifays, U.O. Häfeli, M. Mahmoudi, Crucial ignored parameters on nanotoxicology: the importance of toxicity assay modifications and cell vision, PLoS ONE 7 (1) (2012) e29997.
[29] M. Mahmoudi, A. Simchi, M. Imani, M.A. Shokrgozar, A.S. Milani, U.O. Häfeli, P. Stroeve, A new approach for the in vitro identification of the cytotoxicity of superparamagnetic iron oxide nanoparticles, Colloids Surf. B Biointerfaces 75 (1) (2010) 300–309.
[30] M.P. Monopoli, D. Walczyk, A. Campbell, G. Elia, I. Lynch, F. Baldelli Bombelli, K.A. Dawson, Physical–chemical aspects of protein corona: relevance to in vitro and in vivo biological impacts of nanoparticles, J. Am. Chem. Soc. 133 (8) (2011) 2525–2534.
[31] M. Mahmoudi, S. Laurent, M.A. Shokrgozar, M. Hosseinkhani, Toxicity evaluations of superparamagnetic iron oxide nanoparticles: cell vision versus physicochemical properties of nanoparticles, ACS Nano 5 (9) (2011) 7263–7276.
[32] S. Laurent, C. Burtea, C. Thirifays, U.O. Häfeli, Mahmoudi M, Crucial ignored parameters on nanotoxicology: the importance of toxicity assay modifications and cell vision, PLoS ONE 7 (1) (2012) e29997.
[33] R.W. Paul, A.H.C. Choi, P.W.K. Lee, The α-anomeric form of sialic acid is the minimal receptor determinant recognized by reovirus, Virology 172 (1) (1989) 382–385.
[34] R. Kornfeld, S. Kornfeld, Assembly of asparagine-linked oligosaccharides, Annu. Rev. Biochem. 54 (1) (1985) 631–664.
[35] E. Severi, D.W. Hood, G.H. Thomas, Sialic acid utilization by bacterial pathogens, Microbiology 153 (9) (2007) 2817–2822.
[36] R.E. Schwarz, D.C. Wojciechowicz, A.I. Picon, M.A. Schwarz, P.B. Paty, Wheat-germ agglutinin-mediated toxicity in pancreatic cancer cells, Br. J. Cancer 80 (11) (1999) 1754–1762.